Differential Diffusivity of Nodal and Lefty Underlies a Reaction-Diffusion Patterning System

Patrick Müller *et al.*

Science **336**, 721 (2012);
DOI: 10.1126/science.1221920

Science (print ISSN 0036-8075; online ISSN 1095-9203) is published weekly, except the last week in December, by the American Association for the Advancement of Science, 1200 New York Avenue NW, Washington, DC 20005.

undetectable in chondrocytes; CBFβ is expressed in all cell types at comparable levels (figs. S13 and S14). Fluorescent immunostaining of mouse joint tissue sections also showed coexpression of CBFβ and RUNX1 in cartilage cells (fig. S15). These results are consistent with previous findings about the roles of the genes in chondrogenesis and osteogenesis, and lead us to speculate that RUNX1, rather than RUNX2 or RUNX3, is probably the downstream effector of KGN. When we knocked down RUNX1 expression in hMSCs with shRNAs, KGN-induced chondrocyte differentiation was blocked (fig. S16). Furthermore, *RUNX2* transcription has been shown to be suppressed by RUNX2 through an autoregulation mechanism in different types of cells (*31*). Given the fact that all RUNX family members recognize the same DNA sequence, it is plausible that the RUNX1-CBFβ complex also suppresses *RUNX2* transcription, thus keeping RUNX2 at a relatively low level, which inhibits osteoblast and terminal chondrocyte differentiation.

The development of disease-modifying osteoarthritis drugs has to date focused on (i) slowing the erosion of cartilage by inhibiting matrix-degrading enzymes; (ii) protecting chondrocytes from catabolic activity with antagonists of interleukin-1β and TNF-α or inhibitors of p38, MEK, and caspases; and (iii) the development of anabolic agents, such as FGF18, which promote chondrocyte and chondrocyte progenitor cell proliferation (*3*, *32*, *33*). This work is based on small-molecule effectors of endogenous stem cell populations and may prove synergistic with other efforts currently in development. KGN functions by binding FLNA and disrupting its interaction with CBFβ, which in turn modulates the RUNX family of transcription factors. Recently, two other examples have been reported (*34*, *35*) in which small druglike molecules selectively regulate transcription factor subcellular localization and downstream transcriptional activities. Thus, small molecules appear to be useful tools for selectively modulating gene transcription in cells and whole organisms, and in this case have provided new insights into chondrocyte biology that may lead to novel therapies for the treatment of this degenerative disease.

References and Notes

1. J. Y. Reginster, N. G. Khaltaev, *Rheumatology (Oxford)* **41** (suppl. 1), 1 (2002).
2. M. B. Goldring, S. R. Goldring, *Ann. N.Y. Acad. Sci.* **1192**, 230 (2010).
3. D. J. Hunter, *Nat. Rev. Rheumatol.* **7**, 13 (2011).
4. P. Charbord, *Hum. Gene Ther.* **21**, 1045 (2010).
5. M. F. Pittenger *et al.*, *Science* **284**, 143 (1999).
6. S. P. Grogan, S. Miyaki, H. Asahara, D. D. D'Lima, M. K. Lotz, *Arthritis Res. Ther.* **11**, R85 (2009).
7. S. Koelling *et al.*, *Cell Stem Cell* **4**, 324 (2009).
8. G. N. Smith Jr., *Front. Biosci.* **11**, 3081 (2006).
9. M. Rutgers, D. B. Saris, W. J. Dhert, L. B. Creemers, *Arthritis Res. Ther.* **12**, R114 (2010).
10. S. J. Read, A. Dray, *Expert Opin. Investig. Drugs* **17**, 619 (2008).
11. P. M. van der Kraan, E. L. Vitters, L. B. van de Putte, W. B. van den Berg, *Am. J. Pathol.* **135**, 1001 (1989).
12. S. S. Glasson, T. J. Blanchet, E. A. Morris, *Osteoarthritis Cartilage* **15**, 1061 (2007).
13. K. P. Pritzker *et al.*, *Osteoarthritis Cartilage* **14**, 13 (2006).
14. L. S. Lohmander, T. Saxne, D. K. Heinegård, *Ann. Rheum. Dis.* **53**, 8 (1994).
15. M. Reijman *et al.*, *Arthritis Rheum.* **50**, 2471 (2004).
16. Y. Wang *et al.*, *Oncogene* **26**, 6061 (2007).
17. J. B. Gorlin *et al.*, *J. Cell Biol.* **111**, 1089 (1990).
18. J. T. Connelly, A. J. García, M. E. Levenston, *J. Cell. Physiol.* **217**, 145 (2008).
19. N. Yoshida *et al.*, *Mol. Cell. Biol.* **25**, 1003 (2005).
20. N. Adya, L. H. Castilla, P. P. Liu, *Semin. Cell Dev. Biol.* **11**, 361 (2000).
21. T. Komori, *J. Cell. Biochem.* **112**, 750 (2011).
22. D. Levanon, Y. Groner, *Oncogene* **23**, 4211 (2004).
23. Y. Wang *et al.*, *J. Bone Miner. Res.* **20**, 1624 (2005).
24. S. Wotton *et al.*, *Oncogene* **27**, 5856 (2008).
25. G. S. Stein *et al.*, *Oncogene* **23**, 4315 (2004).
26. T. Komori *et al.*, *Cell* **89**, 755 (1997).
27. F. Otto *et al.*, *Cell* **89**, 765 (1997).
28. S. Kamekura *et al.*, *Arthritis Rheum.* **54**, 2462 (2006).
29. D. Y. Soung *et al*, *J. Bone Miner. Res.* **22**, 1260 (2007).
30. P. M. van der Kraan, E. N. Blaney Davidson, W. B. van den Berg, *Arthritis Res. Ther.* **12**, 201 (2010).
31. H. Drissi *et al.*, *J. Cell. Biochem.* **86**, 403 (2002).
32. M. K. Lotz, V. B. Kraus, *Arthritis Res. Ther.* **12**, 211 (2010).
33. J. Clouet *et al.*, *Drug Discov. Today* **14**, 913 (2009).
34. S. Zhu *et al.*, *Cell Stem Cell* **4**, 416 (2009).
35. H. Wurdak *et al.*, *Proc. Natl. Acad. Sci. U.S.A.* **107**, 16542 (2010).

Acknowledgments: This work was funded by grants from the California Institute for Regenerative Medicine (TR2-01829 to P.G.S.). We are grateful to J. Walker for help in gene expression analysis. Microarray data have been deposited in the National Center for Biotechnology Information's Gene Expression Omnibus with accession number GSE35546. A patent application has been submitted by the authors on the use of kartogenin for chondrogenesis.

Supplementary Materials

www.sciencemag.org/cgi/content/full/science.1215157/DC1
Materials and Methods
Figs. S1 to S16

11 October 2011; accepted 3 March 2012
Published online 5 April 2012;
10.1126/science.1215157

Differential Diffusivity of Nodal and Lefty Underlies a Reaction-Diffusion Patterning System

Patrick Müller,[1]* Katherine W. Rogers,[1] Ben M. Jordan,[2]† Joon S. Lee,[1]† Drew Robson,[1] Sharad Ramanathan,[1,3] Alexander F. Schier[1,3]*

Biological systems involving short-range activators and long-range inhibitors can generate complex patterns. Reaction-diffusion models postulate that differences in signaling range are caused by differential diffusivity of inhibitor and activator. Other models suggest that differential clearance underlies different signaling ranges. To test these models, we measured the biophysical properties of the Nodal/Lefty activator/inhibitor system during zebrafish embryogenesis. Analysis of Nodal and Lefty gradients revealed that Nodals have a shorter range than Lefty proteins. Pulse-labeling analysis indicated that Nodals and Leftys have similar clearance kinetics, whereas fluorescence recovery assays revealed that Leftys have a higher effective diffusion coefficient than Nodals. These results indicate that differential diffusivity is the major determinant of the differences in Nodal/Lefty range and provide biophysical support for reaction-diffusion models of activator/inhibitor-mediated patterning.

In 1952, Alan Turing put forward the reaction-diffusion model, in which two interacting and diffusing species of molecules can generate complex patterns (*1*). Gierer and Meinhardt postulated that pattern formation in reaction-diffusion models requires a short-range activator that enhances both its own production and that of a long-range inhibitor (*2*) (Fig. 1A). Despite the prominence of reaction-diffusion models and the widespread occurrence of short-range activators and long-range inhibitors in development (*3*–*10*), it is unclear how differences in activator and inhibitor ranges arise in vivo. The classic reaction-diffusion models postulate that the inhibitor is more diffusive than the activator (text S1), but more recent studies suggest that differential signal clearance might be a major determinant of differences in signaling range (*11*–*18*) (Fig. 1B). This question has not been resolved because the biophysical properties of diffusion and clearance have not been measured for any activator/inhibitor pair.

The transforming growth factor–β superfamily signals Nodal and Lefty constitute an activator/inhibitor-based system in animals as different as sea urchin and mouse (*3*–*5*, *16*, *18*–*22*) (text S2). Nodals activate signaling during mesendoderm induction and left-right patterning,

[1]Department of Molecular and Cellular Biology, Harvard University, Cambridge, MA 02138, USA. [2]Department of Organismic and Evolutionary Biology, Harvard University, Cambridge, MA 02138, USA. [3]FAS Center for Systems Biology and Harvard Stem Cell Institute, Harvard University, Cambridge, MA 02138, USA.

*To whom correspondence should be addressed. E-mail: pmueller@fas.harvard.edu (P.M.); schier@fas.harvard.edu (A.F.S.)

†These authors contributed equally to this work.

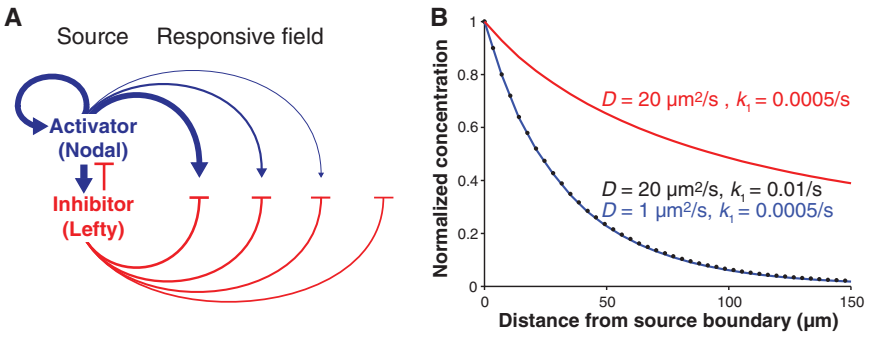

Fig. 1. Model of the Nodal/Lefty activator/inhibitor reaction-diffusion system and regulation of range. (**A**) In the source, Nodal signals (blue) activate their own expression as well as the expression of Lefty (red), which inhibits Nodal production. Nodal signaling in the responsive field is inhibited by the long-range inhibitor Lefty. (**B**) Distribution is controlled by both diffusivity, D, and clearance, k_1. Highly mobile molecules that are rapidly cleared from the extracellular space (black circles) can form gradients similar to those formed by poorly diffusive molecules that are slowly cleared (blue). Decreasing the clearance of the more diffusive species results in a long-range gradient (red). Simulations were performed as described in text S7.

whereas Leftys block pathway activation. The Nodal/Lefty system fulfills two of the tenets of activator/inhibitor reaction-diffusion models: (i) Nodals are short- to mid-range activators that enhance their own expression, and (ii) Leftys are long-range inhibitors that are activated by Nodals (*3*–*5*, *19*, *22*). Genetic and embryological studies in zebrafish have shown that during mesendoderm induction, the two Nodal signals Cyclops and Squint and the two Nodal signaling inhibitors Lefty1 and Lefty2 have different activity ranges: Cyclops is a short-range activator of mesendodermal gene expression, Squint acts at a medium range, and Lefty1 and Lefty2 are long-range inhibitors (*6*, *23*). Moreover, these Nodal signals induce their own expression as well as the expression of Leftys (*5*, *19*, *22*) (Fig. 1A). However, the biophysical properties that control the different activity ranges of Nodals and Leftys are unknown. It therefore remains unclear whether

Fig. 2. Measurement of Nodal-GFP and Lefty-GFP distributions. (**A**) At late blastula stages, about 40 cells secreting Nodal-GFP or Lefty-GFP proteins were transplanted from donor embryos into wild-type hosts (text S4). The gradient profile was determined using a maximum-intensity projection of five confocal slices encompassing a depth of 20 μm (about one cell). (**B**) A representative projection is shown for Squint-GFP. (**C** to **F**) Construct schematic, representative maximum-intensity projection, and distribution profiles 30, 60, and 120 min after transplantation for Cyclops-GFP (C), Squint-GFP (D), Lefty1-GFP (E), and Lefty2-GFP (F). Embryos that did not undergo transplantation were used for background subtraction, and all intensities were normalized to the value most proximal to the source. Error bars indicate SE. Numbers of embryos analyzed at 30, 60, and 120 min after transplantation, respectively: for Cyclops-GFP, $n_{30} = 7$, $n_{60} = 7$, $n_{120} = 7$; for Squint-GFP, $n_{30} = 12$, $n_{60} = 17$, $n_{120} = 20$; for Lefty1-GFP, $n_{30} = 8$, $n_{60} = 8$, $n_{120} = 13$; for Lefty2-GFP, $n_{30} = 12$, $n_{60} = 10$, $n_{120} = 12$.

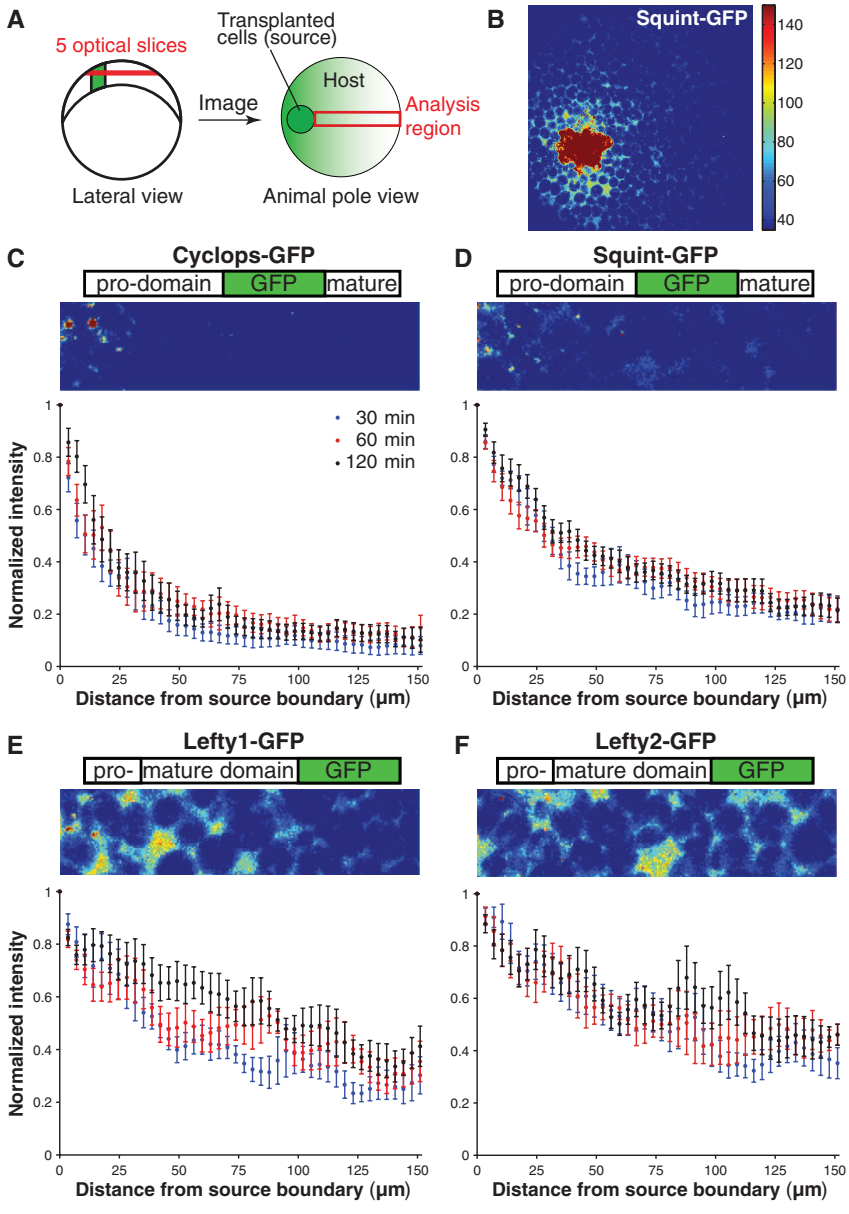

one of the central tenets of reaction-diffusion models—differential diffusivity of activator and inhibitor—is fulfilled in vivo (*4*–*6*, *15*, *16*, *19*, *22*, *24*). To address this question, we performed measurements of Nodal and Lefty distribution, clearance, and diffusivity during zebrafish embryogenesis.

To visualize Nodal and Lefty proteins in vivo, we generated active fusions of green fluorescent protein (GFP) with Cyclops, Squint, Lefty1, and Lefty2 (see figs. S2 to S11 and texts S3 and S4 for analyses of fusion protein activity, processing, localization, and distribution). When expressed from a localized source in blastula embryos, the fusion proteins had activity ranges similar to those of their untagged counterparts (figs. S5 and S10). In vivo imaging revealed that the distribution profiles of the fusion proteins reflected their activity ranges: The gradient formed by Cyclops-GFP exhibited a punctate distribution and dropped steeply as the distance from the source increased, whereas the gradient formed by Squint-GFP was more diffuse and reached farther (Fig. 2, C and 2D). The distributions of Lefty1-GFP and Lefty2-GFP were more shallow and were long-range and super-long-range, respectively (Fig. 2, E and F).

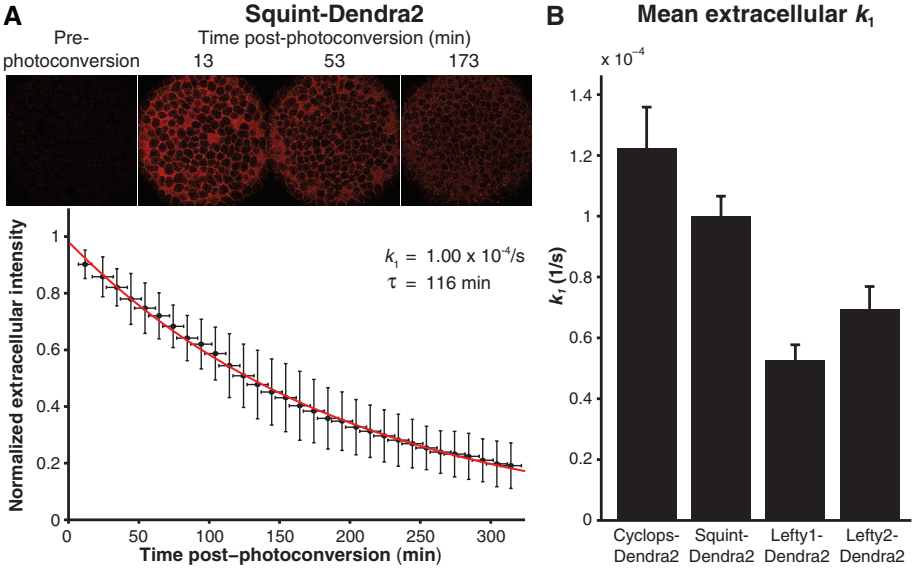

Fig. 3. Measurement of extracellular clearance rate constants. (**A**) Uniformly expressed Nodal-Dendra2 or Lefty-Dendra2 fusion proteins were photoconverted using an ultraviolet pulse. The average extracellular photoconverted Dendra2 intensity was monitored over time and used to determine the clearance rate constants (k_1) and half-lives [$\tau = \ln(2)/k_1$] by fitting exponential functions to data from individual embryos (text S5). The normalized average intensity from Squint-Dendra2 experiments at 10-min intervals (black, $n = 11$) is shown fitted with an exponential function (red). Error bars indicate SD. See fig. S12 for Cyclops-Dendra2, Lefty1-Dendra2, and Lefty2-Dendra2 results. (**B**) Summary of mean extracellular k_1 values. Error bars indicate SE.

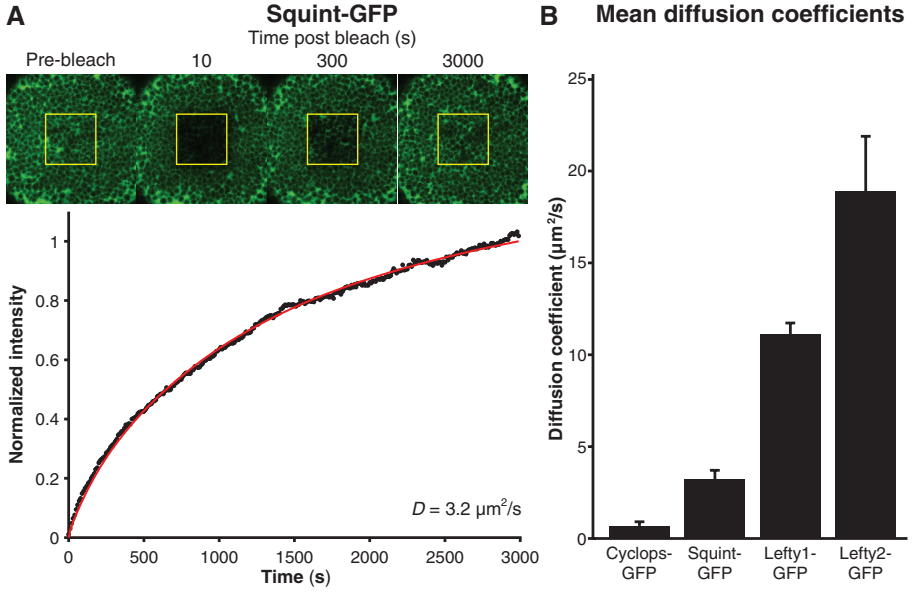

Fig. 4. Measurement of effective diffusion coefficients. (**A**) Uniformly expressed Nodal-GFP or Lefty-GFP fusion proteins were locally photobleached (yellow boxes) at blastula stages. Fluorescence recovery was monitored over time, and the effective diffusion coefficient D was determined by fitting the resulting recovery profile (black) with simulated recovery curves (red) that were numerically generated using a model that includes diffusion, production, and clearance in a three-dimensional embryo-like geometry (text S6). Results for an individual Squint-GFP embryo are shown. See fig. S18 for Cyclops-GFP, Lefty1-GFP, and Lefty2-GFP results. (**B**) Summary of mean diffusion coefficients. Error bars indicate SE.

To determine whether differential clearance underlies the different ranges of Nodal and Lefty signals, we developed a pulse-labeling assay to measure extracellular clearance rate constants. We fused the monomeric green-to-red photoconvertible protein Dendra2 (*25*) to Nodals and Leftys and uniformly expressed these active fusions in blastula embryos (figs. S2 to S10 and text S3). We then switched the fluorescent state of Dendra2 from green to red throughout the embryo and monitored the decrease in intensity of the extracellular red signal for 300 min (Fig. 3 and movie S1). By fitting the data with an exponential decay model, we obtained clearance rate constants (k_1) and calculated the inversely related extracellular half-lives, $\tau = \ln(2)/k_1$ (see figs. S12 to S16 and text S5 for control experiments and detailed measurements). We found half-lives of 95 to 218 min with clearance rate constants of 1.22 (±0.13) × 10^{-4}/s for Cyclops-Dendra2, 1.00 (±0.06) × 10^{-4}/s for Squint-Dendra2, 0.53 (±0.05) × 10^{-4}/s for Lefty1-Dendra2, and 0.69 (±0.07) × 10^{-4}/s for Lefty2-Dendra2 (Fig. 3B and fig. S12). Thus, protein half-lives increased only slightly as ranges increased, which suggests that differential clearance is only a minor contributor to the differences in Nodal and Lefty range.

To determine whether differential diffusivity underlies the different ranges of Nodals and Leftys, we measured their effective diffusion coefficients using fluorescence recovery after photobleaching (FRAP) (*12*, *13*, *18*, *26*). FRAP assays can measure diffusivity over developmentally relevant length and time scales by observing the diffusion-dependent reappearance of fluorescence after photobleaching (text S6). To perform FRAP assays, we ubiquitously expressed Nodal-GFP and Lefty-GFP fusion proteins in blastula embryos and photobleached a cuboidal volume containing several hundred cells. We then monitored the recovery of fluorescence in the bleached region over a period of 50 min (3000 s) (Fig. 4A and figs. S18 to S23). Photobleaching was nearly uniform (fig. S22) and had no apparent toxic effects on the embryo, and fluorescence recovery occurred from regions adjacent to the bleached window (fig. S23). We determined the effective

diffusion coefficients of the fusion proteins by fitting a three-dimensional diffusion model to recovery profiles (text S6 and figs. S19 to S21). We obtained effective diffusion coefficients of $0.7 \pm 0.2\ \mu m^2/s$ for Cyclops-GFP, $3.2 \pm 0.5\ \mu m^2/s$ for Squint-GFP, $11.1 \pm 0.6\ \mu m^2/s$ for Lefty1-GFP, and $18.9 \pm 3.0\ \mu m^2/s$ for Lefty2-GFP (Fig. 4B, figs. S18 to S23, and text S6). Thus, increased protein diffusivities reflect increased ranges, indicating that differential diffusivity is a major contributor to the differences in Nodal and Lefty range.

To test whether the experimentally determined values for diffusivity and clearance accurately predict the measured distribution profiles, we numerically simulated signal secretion from a localized source, diffusion, and clearance (*12*, *14*, *26*) in a three-dimensional geometry appropriate for blastula embryos (text S7). Using the measured values for diffusivity and clearance, these simulations yielded distribution profiles similar to the experimentally determined protein distributions (fig. S26) and thus provided independent support for the validity of the experimental approaches.

Our results have two major implications. First, differential diffusivity underlies differences in activator/inhibitor range. The differences in range (Cyclops < Squint < Lefty1 < Lefty2) are reflected in the differences in effective diffusion coefficients (Cyclops < Squint < Lefty1 < Lefty2). There is a similar trend in half-lives, but the differences in diffusivity are much more pronounced than the differences in clearance. During embryogenesis, the sources of Nodal and Lefty overlap, but Nodal signaling is active near the source and is inhibited by Lefty farther away. Our results suggest that the lower mobility of Nodal allows its accumulation close to the site of secretion, whereas the high mobility of Lefty leads to rapid long-range dispersal and prevents accumulation near the source. Thus, the differential diffusivity of Nodal and Lefty signals serves as the biophysical basis for the spatially restricted induction of cell fates during embryogenesis.

Second, the previously described network topology of the Nodal/Lefty system and the biophysical properties of Nodals and Leftys measured here support the activator/inhibitor reaction-diffusion model of morphogenesis: A less diffusive activator (Nodal) induces both its own production and that of a more diffusive inhibitor (Lefty) (*3*, *4*). The Nodal/Lefty reaction-diffusion system is further constrained by prepatterns and rapid cell fate specification; thus, the system results in graded pathway activation during mesendoderm induction and exclusive pathway activation on the left during left-right specification (see text S2 for detailed discussion). Mathematical models have postulated that the inhibitor in reaction-diffusion systems must have a higher diffusion coefficient than the activator. Several models suggest that clearance-normalized inhibitor and activator diffusion coefficients differ by a factor of at least 6, that is, $\Re = (D/k_1)_{inhibitor}/(D/k_1)_{activator} > 6$ (*8*, *16*, *27*–*29*). The average ratio of the normalized diffusivities of Leftys and Nodals measured here is $\Re \approx 14$, providing biophysical support for these modeling studies (see text S8 for comparison of reaction-diffusion systems). The different diffusivities in the Nodal/Lefty biological system have counterparts in chemical reaction-diffusion systems. For example, patterns can be generated in a starch-loaded gel by combining an activator (iodide) with an inhibitor (chlorite) in the presence of malonic acid (*30*). In this in vitro system, diffusion of the activator is hindered by binding to the starch matrix and is thought to result in a higher (factor of ~15) diffusivity of the inhibitor. These models and our measurements raise the possibility that differential binding interactions and a ratio of at least a factor of 5 to 15 of inhibitor and activator diffusivities might be a general feature of reaction-diffusion–based patterning.

References and Notes

1. A. M. Turing, *Philos. Trans. R. Soc. London Ser. B* **237**, 37 (1952).
2. A. Gierer, H. Meinhardt, *Kybernetik* **12**, 30 (1972).
3. S. Kondo, T. Miura, *Science* **329**, 1616 (2010).
4. H. Meinhardt, *Cold Spring Harb. Perspect. Biol.* **1**, a001362 (2009).
5. H. Shiratori, H. Hamada, *Development* **133**, 2095 (2006).
6. Y. Chen, A. F. Schier, *Curr. Biol.* **12**, 2124 (2002).
7. D. E. Klein, V. M. Nappi, G. T. Reeves, S. Y. Shvartsman, M. A. Lemmon, *Nature* **430**, 1040 (2004).
8. S. Sick, S. Reinker, J. Timmer, T. Schlake, *Science* **314**, 1447 (2006).
9. D. Ben-Zvi, B. Z. Shilo, A. Fainsod, N. Barkai, *Nature* **453**, 1205 (2008).
10. A. D. Economou *et al.*, *Nat. Genet.* **44**, 348 (2012).
11. P. Müller, A. F. Schier, *Dev. Cell* **21**, 145 (2011).
12. A. Kicheva *et al.*, *Science* **315**, 521 (2007).
13. O. Wartlick *et al.*, *Science* **331**, 1154 (2011).
14. S. R. Yu *et al.*, *Nature* **461**, 533 (2009).
15. J. A. Le Good *et al.*, *Curr. Biol.* **15**, 31 (2005).
16. T. Nakamura *et al.*, *Dev. Cell* **11**, 495 (2006).
17. S. Zhou *et al.*, *Curr. Biol.* 10.1016/j.cub.2012.02.065 (2012).
18. K. W. Rogers, A. F. Schier, *Annu. Rev. Cell Dev. Biol.* **27**, 377 (2011).
19. A. F. Schier, *Cold Spring Harb. Perspect. Biol.* **1**, a003459 (2009).
20. V. Duboc, F. Lapraz, L. Besnardeau, T. Lepage, *Dev. Biol.* **320**, 49 (2008).
21. C. Grande, N. H. Patel, *Nature* **457**, 1007 (2009).
22. M. M. Shen, *Development* **134**, 1023 (2007).
23. Y. Chen, A. F. Schier, *Nature* **411**, 607 (2001).
24. L. Marjoram, C. Wright, *Development* **138**, 475 (2011).
25. L. Zhang *et al.*, *Biotechniques* **42**, 446, 448, 450 (2007).
26. T. Gregor, E. F. Wieschaus, A. P. McGregor, W. Bialek, D. W. Tank, *Cell* **130**, 141 (2007).
27. M. I. Granero, A. Porati, D. Zanacca, *J. Math. Biol.* **4**, 21 (1977).
28. S. Kondo, R. Asai, *Nature* **376**, 765 (1995).
29. M. Yamaguchi, E. Yoshimoto, S. Kondo, *Proc. Natl. Acad. Sci. U.S.A.* **104**, 4790 (2007).
30. I. Lengyel, I. R. Epstein, *Science* **251**, 650 (1991).

Acknowledgments: We thank X. Zhang for help with the cloning of Cyclops constructs, H. Othmer and A. Lander for helpful discussions, J. Dubrulle for discussions and primers for quantitative reverse transcription polymerase chain reaction, and S. Mango for comments on the manuscript. Supported by European Molecular Biology Organization and Human Frontier Science Program (HFSP) Long-Term Fellowships (P.M.), the NSF Graduate Research Fellowship Program (K.W.R.), NIH grant 5RO1GM56211, and HFSP grant RGP0066/2004-C.

Supplementary Materials

www.sciencemag.org/cgi/content/full/science.1221920/DC1
Texts S1 to S8
Tables S1 to S8
Figs. S1 to S26
Movie S1
References (*31*–*109*)

14 March 2012; accepted 5 April 2012
Published online 12 April 2012;
10.1126/science.1221920

Mechanical Control of Morphogenesis by Fat/Dachsous/Four-Jointed Planar Cell Polarity Pathway

Floris Bosveld,[1]* Isabelle Bonnet,[1]* Boris Guirao,[1]* Sham Tlili,[1]† Zhimin Wang,[1] Ambre Petitalot,[1] Raphaël Marchand,[1] Pierre-Luc Bardet,[1] Philippe Marcq,[2] François Graner,[1] Yohanns Bellaïche[1]‡

During animal development, several planar cell polarity (PCP) pathways control tissue shape by coordinating collective cell behavior. Here, we characterize by means of multiscale imaging epithelium morphogenesis in the *Drosophila* dorsal thorax and show how the Fat/Dachsous/Four-jointed PCP pathway controls morphogenesis. We found that the proto-cadherin Dachsous is polarized within a domain of its tissue-wide expression gradient. Furthermore, Dachsous polarizes the myosin Dachs, which in turn promotes anisotropy of junction tension. By combining physical modeling with quantitative image analyses, we determined that this tension anisotropy defines the pattern of local tissue contraction that contributes to shaping the epithelium mainly via oriented cell rearrangements. Our results establish how tissue planar polarization coordinates the local changes of cell mechanical properties to control tissue morphogenesis.

Tissue morphogenesis requires the coordination of cell behaviors during development. Planar cell polarity (PCP) pathways, which coordinate the polarization of cells in the tissue plane, have been shown to play a fundamental role in morphogenesis of vertebrates and invertebrates (*1*). It remains largely unknown how PCP pathways control local cell mechan-